Analytically Derived Uplink/Downlink TOA and 2-D-DOA Distributions With Scatterers in a 3-D Hemispheroid Surrounding the Mobile

Andriy Yakovych Olenko, Kainam Thomas Wong, Sajjad Ahmed Qasmi, and Javad Ahmadi-Shokouh

***Abstract*—This paper presents the open literature's first closed-form explicit expressions of the trivariate joint and marginal distributions of a landmobile cellular wireless communication system's uplink and downlink multipaths' time of arrival and two-dimensional direction of arrival, rigorously derived via thorough mathematics based on a "geometrical" model of the three-dimensional (3-D) spatial relationships among the mobile station, the scatterers, and the base station. The scatterers are herein modeled to have a uniform 3-D spatial distribution in an aboveground hemisphere with a flat circular base (or alternatively, within a sphere) centered at the mobile.**

***Index Terms*—Communication channels, dispersive channels, fading channels, geometric modeling, microwave communication, mobile communication, multipath channels, scatter channels.**

I. Analytical Derivation of 3-D TOA/2-D-AOA Distributions

A signal, transmitted from a mobile user in a landmobile radiowave wireless cellular communication system, arrives at the cellular base station through multiple propagation multipaths. Each multipath carries its own propagation history of electromagnetic reflections and diffractions and corruption by multiplicative noise—a history reflected in that multipath's amplitude, Doppler, arrival angle, and arrival time delay at the receiving antenna(s). The values of these amplitudes, Doppler frequency shifts, arrival angles, and arrival time delays depend on the electromagnetic properties of and the spatial geometry among the mobile transmitter, the scatterers, and the receiving antennas. Each receiving antenna's data measurement sums these individually unobservable multipaths.

The time of arrival (TOA)[1] distribution function characterizes the channel's temporal delay spread and frequency incoherence, which in turn determines the obtainable temporal diversity and the extent of intersymbol interference. The two-dimensional (2-D) azimuth-elevation angle of arrival (AOA) determines the angular spread and spatial decorrelation across the spatial aperture of an receiving antenna. The multipaths' nonzero elevation AOAs are most common in urban areas or over hilly terrains or with low-lying receiving antennas, where the propagating wave reflects off vertical structures like buildings or hills. The nonzero elevation AOA is critical for the use of a vertical or planar receiving antenna array, a fact recognized by the European Union's COST Action 259 [19].

"Geometric modeling" idealizes the aforementioned wireless propagation environment via a geometric abstraction of the spatial relationships among the transmitter, the scatterers, and the base station. Geometric models thus attempt to embed measurable fading metrics integrally into the propagation channel's idealized geometry, such that the geometric parameters would affect these various fading metrics in an interconnected manner to reveal conceptually the channel's underlying fading dynamics. This work will maximally embed all derived statistics intrinsically within the propagation channel's geometry and to avoid *a priori ad hoc* statistical assumptions of the received signal's measurable statistics. See [27] for additional discussion on the nature of geometric modeling of wireless propagation.

Geometric modeling contrasts with site-specific/terrain-specific/building-specific empirical measurements or ray-shooting/ray-tracing computer simulations, which are applicable only to the one particular propagation setting under investigation but cannot be easily generalized to wider scenarios. One geometric model can apply for a wide class of propagation settings, producing the received signal's measurable fading metrics (e.g., the uplink and downlink probability density functions of the multipaths' arrival delay and 2-D arrival angle as in this paper) applicable generally within that class of channels.

Geometric modeling contrasts with *ad hoc* nongeometric models that impose certain *ad hoc* and *a priori* statistics separately on individual aspects of the multipaths' spatial and temporal behavior without embedding these side-by-side presumptions into an integrated comprehensive geometric model. Because no underlying geometric interconnection exists in such a nongeometric model, such nongeometric models (perhaps useful as a curve-fitting device) reveal little analytical insight into the propagation channel's fundamental dynamics and offer no conceptual framework to facilitate meaningful generalization into different propagation settings.

Manuscript received May 9, 2004; revised March 19, 2006. This work was supported by Canada's Natural Sciences and Engineering Research Council under Individual Research Grant NSERC-RGPIN-249775-02.

This paper was presented in part at the IEEE Global Telecommunications Conference Dallas, TX, Nov. 29–Dec. 3, 2004.

A. Y. Olenko is with the Department of Probability Theory and Mathematical Statistics, Kyiv University, Kyiv 01033, Ukraine (e-mail: olenk@univ.kiev.ua).

K. T. Wong and J. Ahmadi-Shokouh are with the Department of Electrical and Computer Engineering, University of Waterloo, Waterloo, ON N2L 3G1, Canada (e-mail: ktwong@ieee.org).

S. A. Qasmi is with Sandvine Incorporated, Waterloo, ON N2L 3V3, Canada.

Digital Object Identifier 10.1109/TAP.2006.880661

[1]Also known as the time difference of arrival (TDOA) because this entity describes the propagation delay, not the absolute time.

The mathematically thorough derivation in this paper will rigorously derive the uplink and downlink multipaths' arrival delays and 2-D arrival angles from an idealized geometry, assuming the scatterers to be spatially distributed uniformly within an aboveground hemisphere (or sphere) centered around the mobile but away from the base station.

II. Literature Review on Geometric Modeling for TOA/AOA Distributions

A rich literature exists for rigorous mathematical derivations of the multipaths' TOA and/or AOA distributions based on geometric models, though this literature's overwhelming majority:[2]

1) uses only *two*-dimensional scatterer spatial distributions and is thus limited to the azimuth-only AOA, versus this paper's *three*-dimensional scatterer spatial distribution to derive the 2-D AOA (2-D-AOA) distribution (incorporating both the azimuth and the elevation);
2) focuses on only the uplink, versus both the uplink and the downlink as in this paper;
3) focuses on the *marginal* distributions of either the TOA or the azimuth-only AOA, versus the trivariate and the bivariate (in addition to the univariate) distributions of the TOA and the 2-D-AOA as in this paper.

Only 11 open-literature papers (to the best of the authors' knowledge) have used three-dimensional (3-D) *geometric* models,[3] but none (except [23]) analytically derives closed-form explicit expressions for the TOA-AOA distributions from a geometric model.

1) Only unsolved integral relations for only the spatiotemporal correlation functions are derived in [2], [4], and [25].
2) The vertical-horizontal 2-D spatial correlation is only *computer simulated* via the Monte Carlo method in [3], [12], and [25], with the two former references assuming of the scatterers a cylindrical spatial distribution around the mobile.
3) Closed-form explicit expressions for the Doppler spectrum are analytically derived in [15] based on presumed (and not geometrically derived) azimuth-elevation AOA distributions of the arriving multipaths.
4) Unsolved integral relations for the Doppler spectrum are derived in [6], [25] and for the downlink in [29]. In [6] is one explicit expression applicable to only satellite mobile communications. In [29], the scatterers are modeled as uniformly distributed inside an half-ellipsoid.
5) Unsolved integral equations or summation equations are set up for Monte Carlo simulation characterization of the TOA-AOA statistics in [9] and [22] for *yet-to-be-specified* 3-D scatterer spatial distributions, but no closed-form explicit expressions are analytically derived for the TOA-AOA.
6) Assuming the scatterers as uniformly distributed inside a half-ellipsoid, [23] analytically derives the downlink azimuth-elevation AOA bivariate distribution and the uplink azimuth-AOA univariate marginal distribution as closed-form explicit expressions. Likewise assuming the scatterers as uniformly distributed inside a half-ellipsoid, [29] analytically derives as closed-form explicit expressions the downlink azimuth-AOA univariate distribution, the downlink elevation-AOA univariate distribution, and the downlink spatial cross-correlation coefficient. Neither [23] nor [29] derives any joint involving the TOA or any marginal distribution for TOA. This paper presents complementary results for more generalized metrics, in analytically deriving the uplink's and the downlink's TOA/2-D-AOA's trivariate, bivariate, and univariate distributions; however, [23] allows an elevated base station but this paper does not.

The above literature review thus concludes that this paper is first in the open literature to *analytically* derive via thorough mathematics *closed-form explicit* expressions for:

1) the downlink trivariate distribution of the TOA and 2-D AOA;
2) the uplink trivariate distribution of the TOA and 2-D AOA;
3) the uplink bivariate distribution of the 2-D AOA.

Due to page limitations, these herein-derived results will be compared and contrasted against empirical data in a separate paper.

III. The Proposed New Geometric Model's Assumptions

Fig. 1 shows the 3-D geometry relating the mobile transmitter, the scatterers, and the base station. The mobile is separated from the base stations by the distance D. Though only one scatterer is shown in the figures for graphical clarity, many scatterers exist; and the results herein derived apply to the ensemble of all scatterers. The scatterers are distributed only in a hemispherical spatial region surrounding the mobile transmitter, uniformly with $f^{(he)}(x,y,z) = 3/2\pi R^3$ inside the hemisphere and $f^{(he)}(x,y,z) = 0$ outside. where the spherical radius R is smaller than the distance D between the mobile and the base station.

The subsequent mathematical derivation will be based on these additional propagation-modeling assumptions, made in

[2]Joint TOA/azimuth-AOA distributions (without considering elevation) analytically derived using thorough mathematics from different geometric models of the scatterers' *two*-dimensional spatial locations are available in [5], [18], and [21].

One-dimensional azimuth-AOA marginal distributions (without considering TOA or elevation), likewise analytically derived using thorough mathematics based on various geometric models of the scatterers' 2-D spatial locations, have scatterers modeled as: 1) uniformly distributed only on a uniform circular disc around the mobile in [7], [8], [10], [11], [20]; 2) uniformly distributed only on a uniform hollow-disc around the mobile in [24]; 3) uniformly distributed only on a uniform elliptical disc with foci at the mobile and the base station in [5], [10], [14], [18]; 4) circularly Gaussian distributed centered at the mobile in [16]; and 5) distributed according to an inverted parabola at the mobile in [28].

One-dimensional TOA-only marginal distributions, analytically derived using thorough mathematics based on various geometric models of the scatterers' 2-D spatial locations, can be found in: 1) [13], assuming the scatterers as Rayleigh distributed along any radial axis of a circular disc around the mobile, and 2) [14], assuming the scatterers as uniform distributed over an elliptical disc focused at the base station and the mobile.

[3]Numerous other papers use only *non*geometric or *quasi*-geometric 3-D models that *a priori* impose *ad hoc* statistics on the TOA and the 2-D-AOA, but these statistics are not derived from the geometric relationship among the mobile, the scatterers, and the base station—for example, the nongeometric modeling of the Doppler power spectrum in [1] and [17].

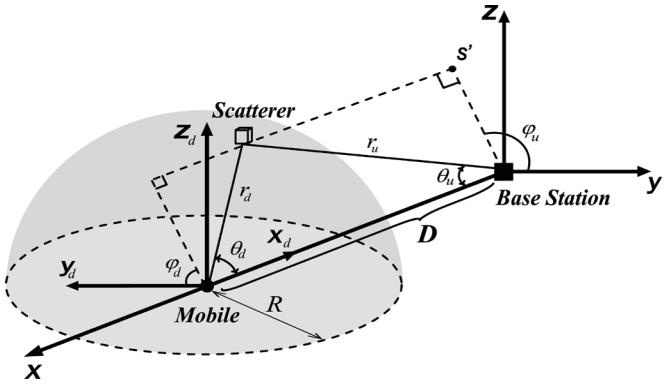

Fig. 1. The proposed hemispherical spatial distributions of scatterers around the mobile, in the uplink/downlink Cartesian/spherical coordinates relating the mobile and an arbitrary scatterer and the base station.

all earlier papers[4] that analytically derived closed-form explicit expressions of the TOA-AOA distributions based on geometrical models.

1) Each propagation path, between the mobile and the base station, reflects off exactly one scatterer. See Fig. 1.
2) Each scatterer acts as an omnidirectional lossless retransmitter, independently of other scatterers.
3) Complex-phase effects in the receiving-antenna's vector summation of the arriving multipaths may be overlooked. That is, all arriving multipaths arriving at each receiving antenna are assumed to be temporally in-phase among themselves.
4) All antennas are isotropic, at both the base station and the mobile.
5) Polarizational effects may be overlooked.

IV. The Uplink Trivariate Joint Distribution of the TOA and the Two-Dimensional DOA

For mathematical convenience, the TOA and 2-D-AOA distributions for the hemispheroid will be derived by considering first a spherical uniform spatial density $f^{(sp)}_{x,y,z}(x,y,z) = 3/4\pi R^3$ inside a sphere of radius R centered at the mobile and $f^{(sp)}_{x,y,z}(x,y,z) = 0$ outside. A spherical distribution of scatterers may seem counterintuitive for its allowance of scatterers located underground; the spherical case is largely used as an intermediate mathematical step. Results from this uplink spherical distribution may be easily transformed to give corresponding results for the uplink hemispherical case as follows.

[4]Namely, [5], [7], [8], [10], [11], [13], [14], [16], [18], [20], [21], [23], [24], and [28].

1) To zero the distribution for all underground azimuth-elevation AOA, i.e., for $\varphi_u \notin [0,\pi]$;
2) To double any distribution parameterized by the φ_u.

However, the spherical model constitutes an alternative geometric model in its right; and this model might be of interest if the mobile is located at some height above the ground.

A. Cartesian-Spherical Coordinates' Transformations

Referring to Fig. 1's spherical coordinates centered at the base station, the ground coincides with the XOY-plane, the mobile is located on the OX-axis, and an arbitrary scatterer has the coordinates (r_u,φ_u,θ_u). These spherical coordinates relate to the Cartesian coordinates (x,y,z) as follows: $(x,y,z) = (r_u\cos\theta_u, r_u\sin\theta_u\cos\varphi_u, r_u\sin\theta_u\sin\varphi_u)$, $r_u^2 = x^2+y^2+z^2$, $\varphi_u = \arctan(z/y)$, $\theta_u = \arccos(x/r_u) = \arccos(x/\sqrt{x^2+y^2+z^2})$, where $r_u \geq 0$, $\theta_u \in [0,\pi]$, $\varphi_u \in [-\pi,\pi)$, Moreover, any Cartesian-defined probability density function may be expressed in the spherical coordinates, shown in (1) at the bottom of the page, where $J(x,y,z)$ symbolizes the Jacobian transformation with

$$J(x,y,z)\big|_{x=r_u\cos\theta_u, y=r_u\sin\theta_u\cos\varphi_u, z=r_u\sin\theta_u\sin\varphi_u} = \begin{vmatrix} \frac{\partial x}{\partial r_u} & \frac{\partial x}{\partial \varphi_u} & \frac{\partial x}{\partial \theta_u} \\ \frac{\partial y}{\partial r_u} & \frac{\partial y}{\partial \varphi_u} & \frac{\partial y}{\partial \theta_u} \\ \frac{\partial z}{\partial r_u} & \frac{\partial z}{\partial \varphi_u} & \frac{\partial z}{\partial \theta_u} \end{vmatrix}^{-1} = -\left[r_u^2\sin\theta_u\right]^{-1}.$$

Fig. 1's spherical coordinates have been chosen to render the Jacobian $J(r_u,\varphi_u,\theta_u)$ independent of φ_u, in order to facilitate the subsequent mathematical derivation of explicit closed-form expressions for the joint and marginal statistics of the TOA and the 2-D AOA. To relate Fig. 1's (r_u,φ_u,θ_u) coordinates to the customary spherical coordinates $(\tilde{r}_u,\tilde{\varphi}_u,\tilde{\theta}_u)$ of Fig. 2, consider the latter's relation to the Cartesian coordinates (x,y,z): $\tilde{r}_u = x^2+y^2+z^2$, $\tilde{\varphi}_u = \arctan(y/x)$, $\tilde{\theta}_u = \arccos(z/\sqrt{x^2+y^2+z^2})$, $x = \tilde{r}_u\sin\tilde{\theta}_u\cos\tilde{\varphi}_u$, $y = \tilde{r}_u\sin\tilde{\theta}_u\sin\tilde{\varphi}_u$, and $z = \tilde{r}_u\cos\tilde{\theta}_u$. Hence, $\tilde{r}_u = r_u$, $\tilde{\varphi}_u = \arctan(\cos\varphi_u\tan\theta_u)$, $\tilde{\theta}_u = \arccos(\sin\theta_u\sin\varphi_u)$, $\varphi_u = \arctan(\cot\tilde{\theta}_u/\sin\tilde{\varphi}_u)$, and $\theta_u = \arccos(\sin\tilde{\theta}_u\cos\tilde{\varphi}_u)$. These relations can convert empirical data collected under Fig. 2's customary coordinates to calibrate the distributions derived under Fig. 1's coordinates, or vice versa.

B. Deriving the Uplink Trivariate Distribution

Towards expressing the trivariate probability density function of (1) in terms of the TOA τ of a multipath (emitted from the

$$f^{(sp)}_{r_u,\varphi_u,\theta_u}(r_u,\varphi_u,\theta_u) = \frac{f^{(sp)}_{x,y,z}(x,y,z)}{|J(x,y,z)|}\Bigg|_{\substack{x=r_u\cos\theta_u \\ y=r_u\sin\theta_u\cos\varphi_u \\ z=r_u\sin\theta_u\sin\varphi_u}} = r_u^2\sin(\theta_u) f^{(sp)}_{x,y,z}(r_u\cos\theta_u, r_u\sin\theta_u\cos\varphi_u, r_u\sin\theta_u\sin\varphi_u) \quad (1)$$

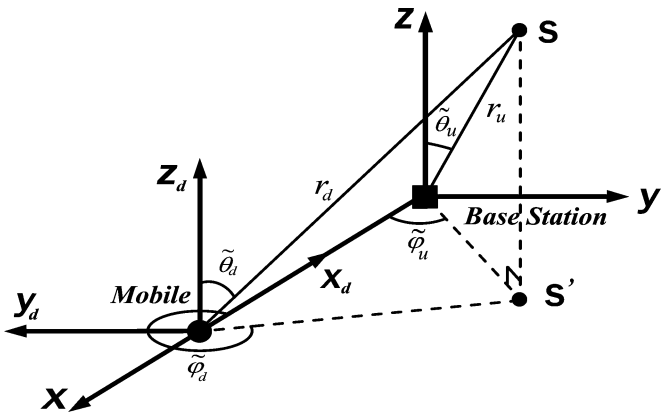

Fig. 2. The customary spherical coordinates relating the mobile, a scatterer, and the base station.

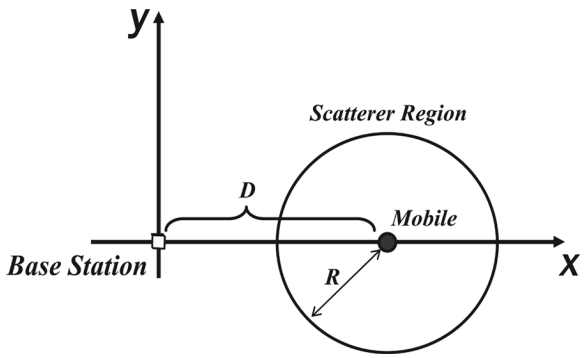

Fig. 3. Projection of the 3-D figure onto the 2-D XOY-plane, using the former's invariance with respect to φ_u.

mobile, reflecting off a scatterer, and arriving at the base station), r_u from Fig. 1's geometry may be related to the TOA τ as follows:

$$\tau = \frac{r_u + r_d}{c} = \frac{r_u + \sqrt{D^2 + r_u^2 - 2r_u D\cos\theta_u}}{c}$$
$$r_u = D\bar{r}_u = \frac{D}{2}\frac{1-\left(\frac{\tau c}{D}\right)^2}{\cos\theta_u - \frac{\tau c}{D}}$$

where c denotes light speed

$$J(r_u,\varphi_u,\theta_u) = \left|\frac{dr_u}{d\tau}\right|^{-1} = \frac{2}{c}\frac{\left(\cos\theta_u - \frac{\tau c}{D}\right)^2}{1+\left(\frac{\tau c}{D}\right)^2 - 2\frac{\tau c}{D}\cos\theta_u}.$$

Hence, (1) becomes (2), shown at the bottom of the page, where

$$A_u = \frac{1+\left(\frac{\tau c}{D}\right)^2 - 2\frac{\tau c}{D}\cos\theta_u}{2\left(\frac{\tau c}{D} - \cos\theta_u\right)}. \tag{3}$$

As Fig. 1's coordinates have been defined such that the spherical density is invariant with respect to any rotation around the axis OX (i.e., any change in φ_u), only the 2-D projection in Fig. 3 need be considered to define the exact support region wherein the trivariate distribution in (2) may be nonzero. That gives the constraint

$$r_u^2 - 2r_u D\cos\theta_u + D^2 \le R^2$$
$$\Rightarrow \quad A_u \le \frac{R}{D}. \tag{4}$$

The special case of $(\theta_u,\tau) = (0,(D/c))$ produces 0/0 in (3) and needs separate consideration; this corresponds to a direct propagation from the mobile to the base station without reflection off any scatterer or only off scatterers on the OX axis.

$$1 \le \frac{\tau c}{D} \le 1 + \frac{2R}{D}. \tag{5}$$

When (5) is false, τ would correspond to a hypothetical scattering location outside the scatterers' spherical support region, hence $f^{(sp)}_{\tau,\varphi_u,\theta_u}(\tau,\varphi_u,\theta_u) = 0$.

To conclude

$$f^{(sp)}_{\tau,\varphi_u,\theta_u}(\tau,\varphi_u,\theta_u) = \begin{cases} \frac{3A_u(c/D)\bar{r}_u^2\sin\theta_u}{4\pi\left(\frac{R}{D}\right)^3\left(\frac{\tau c}{D}-\cos\theta_u\right)}, & \text{if } \theta_u \ne 0 \text{ and } A_u \le \frac{R}{D} \\ 0, & \text{otherwise.} \end{cases}$$

$$\begin{aligned} f^{(sp)}_{\tau,\varphi_u,\theta_u}(\tau,\varphi_u,\theta_u) &= \left.\frac{f^{(sp)}_{r_u,\varphi_u,\theta_u}(r_u,\varphi_u,\theta_u)}{|J(r_u,\varphi_u,\theta_u)|}\right|_{r_u=\frac{D}{2}\frac{1-\left(\frac{\tau c}{D}\right)^2}{\cos\theta_u-\frac{\tau c}{D}}} \\ &= \frac{A_u}{\frac{\tau c}{D}-\cos\theta_u} f^{(sp)}_{r_u,\varphi_u,\theta_u}(r_u,\varphi_u,\theta_u) \\ &= \frac{A_u c r_u^2\sin\theta_u}{\frac{\tau c}{D}-\cos\theta_u} f^{(sp)}_{x,y,z}(r_u\cos\theta_u, r_u\sin\theta_u\cos\varphi_u, r_u\sin\theta_u\sin\varphi_u) \end{aligned} \tag{2}$$

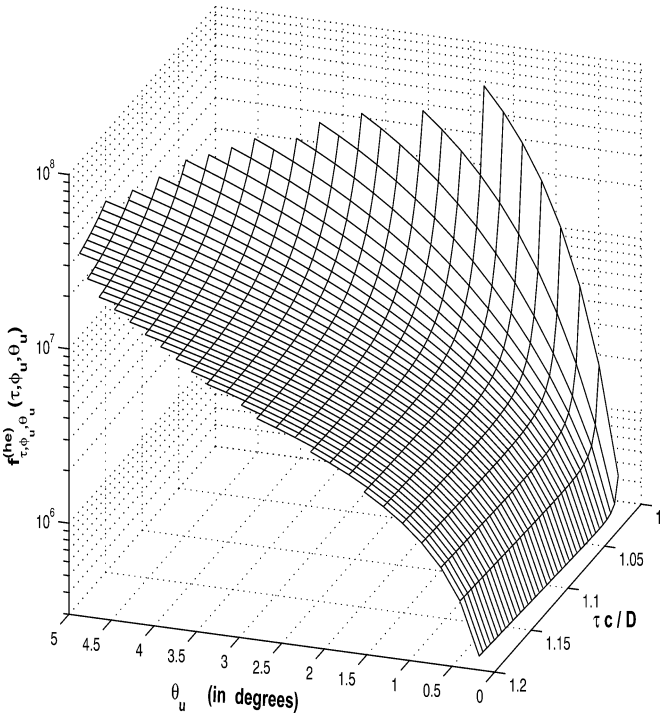

Fig. 4. The uplink trivariate TOA/2-D-AOA distribution for a hemispheroid scattering region around the mobile, with $D = 1000$ m and $R = 100$ m.

Applying the two-step procedure at the start of Section IV, the trivariate TOA/2-D-AOA distribution for the hemispherical scatterers case equals

$$f^{(he)}_{\tau,\varphi_u,\theta_u}(\tau,\varphi_u,\theta_u)=\begin{cases}\frac{3A_u(c/D)\bar{r}_u^2\sin\theta_u}{2\pi\left(\frac{R}{D}\right)^3\left(\frac{\tau c}{D}-\cos\theta_u\right)}, & \text{if } \theta_u\neq 0, A_u\leq\frac{R}{D} \\ & \text{and } 0\leq\varphi_u\leq\pi \\ 0, & \text{otherwise.}\end{cases} \tag{6}$$

The above two equations have specified no value to $f^{(sp)}_{\tau,\varphi_u,\theta_u}(\tau,\varphi_u,\theta_u)$ and $f^{(he)}_{\tau,\varphi_u,\theta_u}(\tau,\varphi_u,\theta_u)$ at $\theta_u = 0$, noting the above expressions at $\theta_u = 0$ would lead to a 0/0 situation. Any arbitrary finite nonnegative value may be assigned to $f^{(sp)}_{\tau,\varphi_u,\theta_u}(\tau,\varphi_u,\theta_u)$ and $f^{(he)}_{\tau,\varphi_u,\theta_u}(\tau,\varphi_u,\theta_u)$ at $\theta_u = 0$, and the overall distribution will still integrate to unity over the entire trivariate support region over $(\tau,\varphi_u,\theta_u)$. Also, when either trivariate distribution is nonzero, it is not a function of φ_u.

Equation (6) is plotted in Fig. 4 for $D = 1000$ m and $R = 100$m. As θ_u increases, the involved scatterers are those closer to the hemispheroid's top. The scatterers producing the longest (shortest) delays are those farthest from (closest to) the base station and located near the hemispheroid's flat bottom (i.e., with near-zero θ_u). Hence, the support region of (6) fans out wider to the right but narrows to a tip at center left in Fig. 4.

V. The Uplink Bivariate Joint Distributions

A. Deriving the Uplink 2-D-AOA Joint Distribution

To obtain the 2-D-AOA joint distribution of (φ_u,θ_u), the trivariate distribution of (r_u,φ_u,θ_u) is to be integrated with respect to r_u. Fixing φ_u gives a plane; further fixing θ_u gives a line on this plane. The smallest and the largest values of r_u where the aforementioned line intersects the scattering sphere equals

$$\underline{r}(\theta_u)=D\left[\cos\theta_u-\sqrt{\left(\frac{R}{D}\right)^2-\sin^2\theta_u}\right]$$
$$\overline{r}(\theta_u)=D\left[\cos\theta_u+\sqrt{\left(\frac{R}{D}\right)^2-\sin^2\theta_u}\right].$$

The above may be more easily seen by considering the scattering sphere's projection on the by-plane, namely, the circle in Fig. 3 defined by

$$r_u^2-2-D\cos\theta_u r_u+D^2-R^2=0. \tag{7}$$

Hence

$$\begin{aligned}
&f^{(sp)}_{\varphi_u,\theta_u}(\varphi_u,\theta_u)\\
&\quad=\int_{\frac{D}{c}}^{\frac{D+2R}{c}} f^{(sp)}_{\tau,\varphi_u,\theta_u}(\tau,\varphi_u,\theta_u)d\tau\\
&\quad=\int_{\underline{r}(\theta_u)}^{\overline{r}(\theta_u)} r_u^2\sin(\theta_u)f(r_u\cos\theta_u,r_u\sin\theta_u\cos\varphi_u,\\
&\qquad\qquad r_u\sin\theta_u\sin\varphi_u)dr_u\\
&\quad=\frac{\sin\theta_u}{\frac{4}{3}\pi R^3}\int_{\underline{r}(\theta_u)}^{\overline{r}(\theta_u)} r_u^2dr_u\\
&\quad=\frac{1}{2\pi}\left(\frac{R}{D}\right)^{-3}\left\{\left[4\cos^2\theta_u+\left(\frac{R}{D}\right)^2-1\right]\right.\\
&\qquad\qquad\left.\sin\theta_u\sqrt{\left(\frac{R}{D}\right)^2-\sin^2\theta_u}\right\}
\end{aligned}$$

for $\theta_u \in [0,\arcsin(R/D)]$ and $\varphi_u \in [0,2\pi)$. Otherwise $f^{(sp)}_{\varphi_u,\theta_u}(\varphi_u,\theta_u)=0$.

The corresponding distribution for the hemispherical scatterers case equals (8) as shown at the bottom of the page.When

$$f^{(he)}_{\varphi_u,\theta_u}(\varphi_u,\theta_u)=\begin{cases}\frac{1}{\pi}\left(\frac{R}{D}\right)^{-3}\left\{\left[4\cos^2\theta_u+\left(\frac{R}{D}\right)^2-1\right]\sin\theta_u\sqrt{\left(\frac{R}{D}\right)^2-\sin^2\theta_u}\right\} & \text{if } \theta_u\in\left[0,\arcsin\left(\frac{R}{D}\right)\right] \text{ and } 0\leq\varphi_u\leq\pi \\ 0, & \text{otherwise}\end{cases} \tag{8}$$

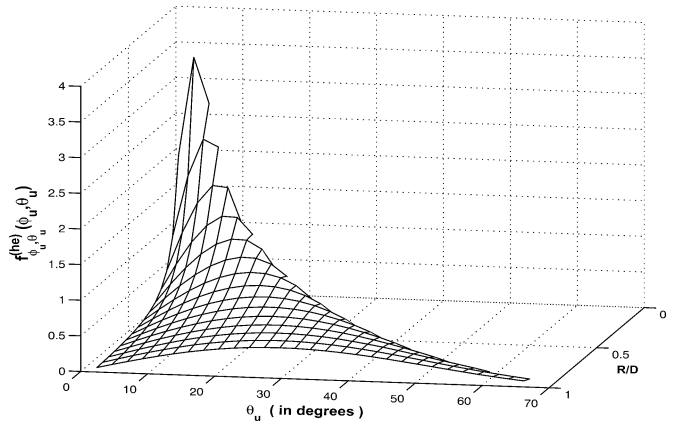

Fig. 5. The uplink azimuth elevation 2-D AOA bivariate distribution.

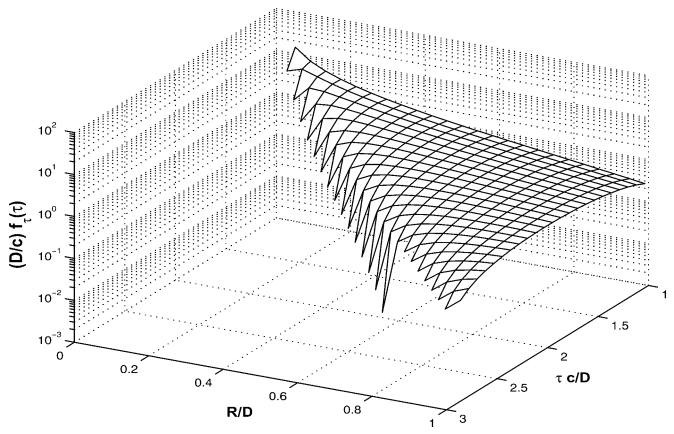

Fig. 6. The uplink or downlink TOA distribution.

either bivariate 2-D-AOA distribution is nonzero, it is not a function of φ_u.

Equation (8) is plotted in Fig. 5 versus various values of θ_u and R/D. As the scattering hemispheroid gets smaller relative to its distance from the base station, R/D approaches zero, and all scatterers look to the base station as less spread out over the azimuth but more limited in elevation to near the horizon. Hence, (8) is limited to a smaller support range for θ_u, as R/D decreases.

The above-derived uplink 2-D-AOA's bivariate distribution concurs with that derived in [23], after adjustments between the different used coordinates.[5]

B. Deriving the Uplink Joint Distribution of τ and φ_u

From (7)

$$\cos\theta_u = \frac{r_u^2 + D^2 - R^2}{2Dr_u} = \frac{1}{2}\frac{\left(\frac{\tau c}{D}\right)^2 - 2\frac{\tau c}{D}\frac{R}{D} + 1}{\frac{\tau c}{D} - \frac{R}{D}}$$

[5]Reference [23] uses the coordinates in Fig. 2, whereas the derivation in this paper uses the coordinates in Fig. 1. The coordinates in this paper allow the derivation of closed-form explicit expressions for the uplink's 2-D-AOA's joint bivariate distributions, as well as the uplink's and the downlink's trivariate TOA/2-D-AOA distributions.

with $r_u = \tau c - R$ for points on a spherical surface with radius R in Fig. 1. Hence, $f^{(sp)}_{\tau,\varphi_u,\theta_u}(\tau,\varphi_u,\theta_u)$ effectively needs integration with respect to θ_u from zero to

$$\theta_1 = \arccos\left[\frac{1}{2}\frac{\left(\frac{\tau c}{D}\right)^2 - 2\frac{\tau c}{D}\frac{R}{D} + 1}{\frac{\tau c}{D} - \frac{R}{D}}\right].$$

That is, with $u = \cos\theta_u$ and $Du - \tau c = x$

$$\begin{aligned}
f^{(sp)}_{\tau,\varphi_u}(\tau,\varphi_u) &= \int_0^{\pi} f^{(sp)}_{\tau,\varphi_u,\theta_u}(\tau,\varphi_u,\theta_u)d\theta_u \\
&= \int_0^{\theta_1} \frac{3}{32}\frac{c}{D}\frac{\left[1-\left(\frac{\tau c}{D}\right)^2\right]^2}{\pi\left(\frac{R}{D}\right)^3} \\
&\quad \sin\theta_u \frac{1+\left(\frac{\tau c}{D}\right)^2 - 2\left(\frac{\tau c}{D}\right)\cos\theta_u}{\left(\cos\theta_u - \frac{\tau c}{D}\right)^4}d\theta_u \\
&= \frac{3}{32}\frac{c}{D}\frac{\left[1-\left(\frac{\tau c}{D}\right)^2\right]^2}{\pi\left(\frac{R}{D}\right)^3} \int_{\cos\theta_1}^{1} \frac{1+\left(\frac{\tau c}{D}\right)^2 - 2u\frac{\tau c}{D}}{\left(u-\frac{\tau c}{D}\right)^4}du \\
&= \frac{3}{32}\frac{c}{D}\frac{\left[1-\left(\frac{\tau c}{D}\right)^2\right]^2}{\pi\left(\frac{R}{D}\right)^3} \int_{D\cos\theta_1-\tau c}^{D-\tau c} D^3\frac{1-\left(\frac{\tau c}{D}\right)^2}{x^4}dx \\
&\quad - \frac{3}{32}\frac{c}{D}\frac{\left[1-\left(\frac{\tau c}{D}\right)^2\right]^2}{\pi\left(\frac{R}{D}\right)^3} \int_{D\cos\theta_1-\tau c}^{D-\tau c} \frac{2 - D^2\left(\frac{\tau c}{D}\right)}{x^3}dx.
\end{aligned}$$

Hence, for $\tau \in [(D/c);(D+2R/c)]$ and $\varphi_u \in [0, 2\pi)$

$$f^{(sp)}_{\tau,\varphi_u}(\tau,\varphi_u) = \frac{c/D}{32\pi\left(\frac{R}{D}\right)^3}\left\{12\frac{c\tau}{D}\left(\frac{R}{D}\right)^2 - 8\left(\frac{R}{D}\right)^3 + 3\left(\frac{c\tau}{D}\right)^2 - 2\left(\frac{c\tau}{D}\right)^3 - 1\right\}$$

otherwise, $f^{(sp)}_{\tau,\varphi_u}(\tau,\varphi_u) = 0$.

The corresponding distribution for the hemispherical scatterers case equals

$$f^{(he)}_{\tau,\varphi_u}(\tau,\varphi_u) = \begin{cases} \frac{c}{D}\frac{12\frac{c\tau}{D}\left(\frac{R}{D}\right)^2 - 8\left(\frac{R}{D}\right)^3 + 3\left(\frac{c\tau}{D}\right)^2 - 2\left(\frac{c\tau}{D}\right)^3 - 1}{16\pi\left(\frac{R}{D}\right)^3}, & \text{if } \tau \in \left[\frac{D}{c};\frac{D+2R}{c}\right], \\ & \text{and } 0 \le \varphi_u \le \pi \\ 0, & \text{otherwise.} \end{cases} \tag{9}$$

When either bivariate distribution is nonzero, it is not a function of φ_u; hence, it has the same shape in Fig. 6, to be discussed later.

C. Deriving the Uplink Joint Distribution of τ and θ_u

Because the trivariate $f^{(sp)}_{\tau,\varphi_u,\theta_u}(\tau,\varphi_u,\theta_u)$ does not depend on φ_u, the bivariate $f^{(sp)}_{\tau,\theta_u}(\tau,\theta_u)$ simply equals the former multiplied by 2π

$$f^{(sp)}_{\tau,\theta_u}(\tau,\theta_u)=\begin{cases}\frac{3A_u(c/D)\bar{r}_u^2\sin\theta_u}{2\left(\frac{R}{D}\right)^3\left(\frac{\tau c}{D}-\cos\theta_u\right)}, & \text{if } \theta_u\in(0,\pi], A_u\le\frac{R}{D} \\ & \text{and } \tau\in\left[\frac{D}{c},\frac{D+2R}{c}\right] \\ 0, & \text{otherwise}\end{cases}$$
$$=f^{(he)}_{\tau,\theta_u}(\tau,\theta_u) \tag{10}$$

which is a π-multiple of (6) and thus follows the same trends as Fig. 4.

VI. The Uplink Marginal Densities, Means, and Standard Deviations

A. Deriving the Marginal Statistics of τ

Integration of $f^{(sp)}_{\tau,\varphi_u}(\tau,\varphi_u)$ with respect to $\varphi_u\in[-\pi,\pi)$ gives, for $\tau\in[(D/c),(D+2R/c)]$

$$f^{(sp)}_{\tau}(\tau)=\int_{-\pi}^{\pi}f^{(sp)}_{\tau,\varphi_u}(\tau,\varphi_u)d\varphi_u$$
$$=\frac{c/D}{16\left(\frac{R}{D}\right)^3}\left\{12\frac{c\tau}{D}\left(\frac{R}{D}\right)^2-8\left(\frac{R}{D}\right)^3+3\left(\frac{c\tau}{D}\right)^2-2\left(\frac{c\tau}{D}\right)^3-1\right\}$$
$$=f^{(he)}_{\tau}(\tau). \tag{11}$$

Otherwise, $f^{(sp)}_{\tau}(\tau)=f^{(he)}_{\tau}(\tau)=0$.

Hence, the expectation and variance of τ equal, respectively

$$E[\tau]=\int_{\frac{D}{c}}^{\frac{D+2R}{c}}\tau f^{(sp)}_{\tau}(\tau)d\tau$$
$$=\frac{D}{c}\left[1+\frac{3}{4}\frac{R}{D}+\frac{1}{5}\left(\frac{R}{D}\right)^2\right]$$
$$D[\tau]=\int_{\frac{D}{c}}^{\frac{D+2R}{c}}\tau^2 f^{(sp)}_{\tau}(\tau)d\tau-\left(E^{(sp)}[\tau]\right)^2$$
$$=\left(\frac{D}{c}\right)^2\left[\frac{19}{80}\left(\frac{R}{D}\right)^2+\frac{1}{30}\left(\frac{R}{D}\right)^3-\frac{1}{25}\left(\frac{R}{D}\right)^4\right].$$

The root-mean-square (rms) TOA equals

$$\tau_{\mathrm{RMS}}=\sqrt{D[\tau]+(E[\tau])^2}$$
$$=\frac{D}{c}\sqrt{1+\frac{3}{2}\frac{R}{D}+\frac{6}{5}\left(\frac{R}{D}\right)^2+\frac{1}{3}\left(\frac{R}{D}\right)^3}. \tag{12}$$

$f^{(he)}_{\tau}(\tau)$ and τ_{RMS} are, respectively, plotted in Figs. 6 and 7. $f^{(he)}_{\tau}(\tau)$, plotted in Fig. 6, has a $(\tau c/D,\theta_u)$ support region with trends similar to $f^{(he)}_{\varphi_u,\theta_u}(\varphi_u,\theta_u)$ in Fig. 5. τ_{RMS}, as expected, increases as D increases. However, τ_{RMS} also increases slightly as R/D increases even if D remains constant because the higher values of τ more than counterbalance its lower values in the square operation in computing τ_{RMS}.

B. Deriving the Marginal Statistics of φ_u

As $f^{(sp)}_{\varphi_u}(\varphi_u)$ is invariant over φ_u

$$f^{(sp)}_{\varphi_u}(\varphi_u)=\begin{cases}\frac{1}{2\pi}, & \text{if } \varphi_u\in[-\pi,\pi) \\ 0, & \text{else.}\end{cases}$$

The above uniform distribution gives

$$E^{(sp)}[\varphi_u]=\int_{-\pi}^{\pi}\varphi_u f^{(sp)}_{\varphi_u}(\varphi_u)d\varphi_u=0$$
$$D^{(sp)}[\varphi_u]=\int_{-\pi}^{\pi}\varphi_u^2 f^{(sp)}_{\varphi_u}(\varphi_u)d\varphi_u-\left(E^{(sp)}[\varphi_u]\right)^2=\frac{\pi^2}{3}.$$

The corresponding distribution for the hemispherical scatterers case equals

$$f^{(he)}_{\varphi_u}(\varphi_u)=\begin{cases}\frac{1}{\pi}, & \text{if } \varphi_u\in[0,\pi] \\ 0, & \text{else}\end{cases}$$
$$E^{(he)}[\varphi_u]=\pi/2$$
$$D^{(he)}[\varphi_u]=\frac{\pi^2}{12}. \tag{13}$$

C. Deriving the Marginal Statistics of θ_u

See (14) and (15) at the bottom of the page. $E^{(he)}[\theta_u]=E^{(sp)}[\theta_u]$ and $D^{(sp)}[\theta_u]=D^{(he)}[\theta_u]$ cannot be expressed in a closed form.

VII. Downlink TOA and 2-D-AOA Joint/Marginal Distributions

Under the Cartesian coordinates (x_d,y_d,z_d) in Fig. 1 centered at the mobile, $f^{(sp)}_{r_d,\theta_d,\varphi_d}(r_d,\theta_d,\varphi_d)$ takes the same mathematical form as $f^{(sp)}_{r_u,\theta_u,\varphi_u}(r_u,\theta_u,\varphi_u)$ (but with the subscripts

$$f^{(sp)}_{\theta_u}(\theta_u)=\int_{-\pi}^{\pi}f^{(sp)}_{\varphi_u,\theta_u}(\varphi_u,\theta_u)d\varphi_u$$
$$=\begin{cases}\frac{\left[4\cos^2\theta_u+\left(\frac{R}{D}\right)^2-1\right]\sin\theta_u\sqrt{\left(\frac{R}{D}\right)^2-\sin^2\theta_u}}{\left(\frac{R}{D}\right)^3}, & \text{if } \theta_u\in\left[0,\arcsin\left(\frac{R}{D}\right)\right] \\ 0, & \text{else}\end{cases} \tag{14}$$
$$=f^{(he)}_{\theta_u}(\theta_u) \tag{15}$$

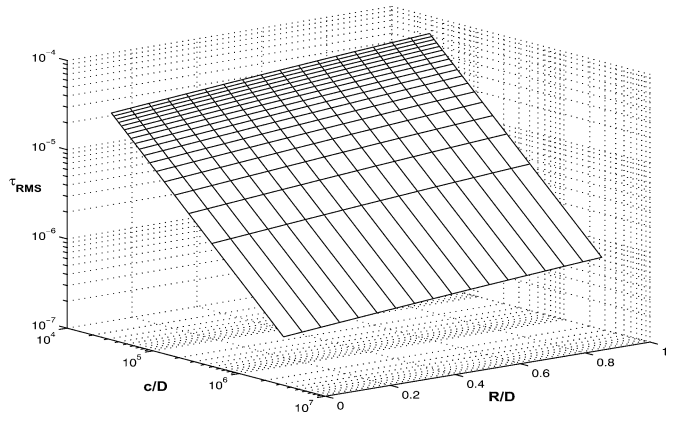

Fig. 7. The uplink or downlink rms TOA.

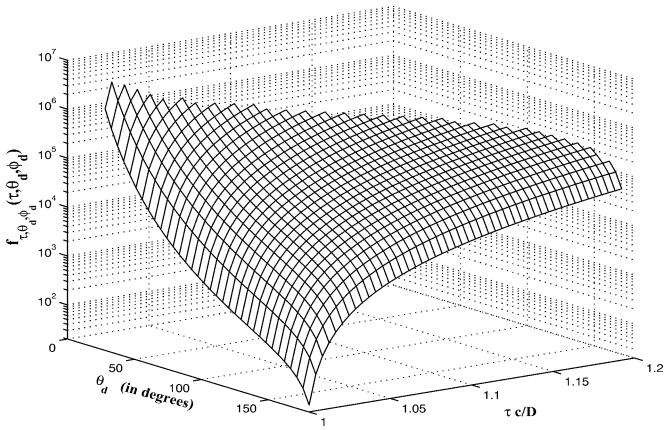

Fig. 8. The downlink trivariate distribution of the TOA and the azimuth-elevation 2-D AOA for a hemispheroid scattering region around the mobile, with $D = 1000$ m and $R = 100$ m.

d replacing u). This is because the same transformation of coordinates holds for the uplink and for the downlink and because $f^{(sp)}_{x,y,z}(x,y,z)$ takes on only binary values. The difference is only in their respective support regions of nonzero values; the uplink has (4), whereas the downlink has

$$\bar{r}_d = \frac{r_d}{D} = \frac{1}{2}\frac{1-\left(\frac{\tau c}{D}\right)^2}{\cos\theta_d - \frac{\tau c}{D}} < \frac{R}{D}.$$

Results from the downlink spherical distribution may be easily transformed to give corresponding results for the downlink hemispherical case, similar to the uplink case.

The downlink's trivariate TOA/2-D-AOA distributions thus equal

$$f^{(sp)}_{\tau,\varphi_d,\theta_d}(\tau,\varphi_d,\theta_d) = \begin{cases} \frac{3A_d(c/D)\bar{r}_d^2\sin\theta_d}{4\pi\left(\frac{R}{D}\right)^3\left(\frac{\tau c}{D}-\cos\theta_d\right)}, & \text{if } \bar{r}_d \le \frac{R}{D}, \theta_d \in (0,\pi] \\ & \quad \text{and } \varphi_d \in [-\pi,\pi) \\ 0, & \text{otherwise} \end{cases} \tag{16}$$

$$f^{(he)}_{\tau,\varphi_d,\theta_d}(\tau,\varphi_d,\theta_d) = \begin{cases} \frac{3A_d(c/D)\bar{r}_d^2\sin\theta_d}{2\pi\left(\frac{R}{D}\right)^3\left(\frac{\tau c}{D}-\cos\theta_d\right)}, & \text{if } \bar{r}_d \le \frac{R}{D}, \theta_d \in (0,\pi] \\ & \quad \text{and } \varphi_d \in [0,\pi] \\ 0, & \text{otherwise} \end{cases} \tag{17}$$

where

$$A_d = \frac{1+\left(\frac{\tau c}{D}\right)^2 - 2\frac{\tau c}{D}\cos\theta_d}{2\left(\frac{\tau c}{D}-\cos\theta_d\right)}.$$

As in the uplink case, the above two equations have not specified any value to $f^{(sp)}_{\tau,\varphi_d,\theta_d}(\tau,\varphi_d,\theta_d)$ and $f^{(he)}_{\tau,\varphi_d,\theta_d}(\tau,\varphi_d,\theta_d)$ at $\theta_d = 0$, noting $\theta_d = 0$ leads to a 0/0 situation in the above expressions. Any arbitrary finite nonnegative value may be assigned to $f^{(sp)}_{\tau,\varphi_d,\theta_d}(\tau,\varphi_d,\theta_d)$ and $f^{(he)}_{\tau,\varphi_d,\theta_d}(\tau,\varphi_d,\theta_d)$ at $\theta_d = 0$, and the overall distribution will still integrate to unity over the entire trivariate support region over $(\tau,\varphi_d,\theta_d)$. Moreover, when either above trivariate distribution is nonzero, it is not a function of φ_d. These downlink trivariate distributions are identical in mathematical form but different in support region as their uplink counterparts. Plotted in Fig. 8 is (17) at $D = 1000$ m and $R = 100$ m.

Under the Cartesian coordinates (x_d, y_d, z_d) in Fig. 1 centered at the mobile, the scatterer's spherical spatial distribution

$$f^{(sp)}_{x_d,y_d,z_d}(x_d,y_d,z_d) = \begin{cases} \frac{3}{4\pi R^3}, & \text{if } x_d^2+y_d^2+z_d^2 \le R^2 \\ 0, & \text{otherwise} \end{cases}$$

remains invariant for any rotation around the origin. Hence, the downlink trivariate TOA/2-D-AOA distribution would stay invariant for any shift in θ_d or φ_d. The scatterers' symmetry around the mobile implies φ_d-invariance:

$$f^{(sp)}_{\varphi_d}(\varphi_d) = \begin{cases} \frac{1}{2\pi}, & \text{if } \varphi_d \in [-\pi,\pi) \\ 0, & \text{otherwise} \end{cases}$$
$$f^{(he)}_{\varphi_d}(\varphi_d) = \begin{cases} \frac{1}{\pi}, & \text{if } \varphi_d \in [0,\pi] \\ 0, & \text{otherwise.} \end{cases} \tag{18}$$

Moreover, integrating the above trivariate TOA/2-D-AOA distributions with respect to φ_d gives

$$f^{(sp)}_{\tau,\theta_d}(\tau,\theta_d) = \begin{cases} \frac{3A_{1d}(c/D)\bar{r}_d^2\sin\theta_d}{2\left(\frac{R}{D}\right)^3\left(\frac{\tau c}{D}-\cos\theta_d\right)}, & \text{if } \theta_d \in (0,\pi], \tau \in \left[\frac{D}{c}, \frac{D+2R}{c}\right] \\ & \quad \text{and } \bar{r}_d \le \frac{R}{D} \\ 0, & \text{otherwise} \end{cases}$$
$$= f^{(he)}_{\tau,\theta_d}(\tau,\theta_d) \tag{19}$$

which simply equals a π-multiple of (17).

As the propagation delay is invariant to the propagation's direction, the downlink arrival delay's distribution remains same as the uplink's $f^{(sp)}_{\tau}(\tau)$ and $f^{(he)}_{\tau}(\tau)$, respectively, for the spherical and the hemispherical scatterer geometries

$$f^{(sp)}_{\tau,\varphi_d}(\tau,\varphi_d) = \frac{1}{2\pi}f^{(sp)}_{\tau}(\tau), \quad \forall\varphi_d \in [-\pi,\pi)$$
$$= f^{(he)}_{\tau,\varphi_d}(\tau,\varphi_d). \tag{20}$$

When either above bivariate distribution is nonzero, it is not a function of φ_d

$$f^{(sp)}_{\theta_d,\varphi_d}(\theta_d,\varphi_d) = \int_0^R f^{(sp)}_{r_d,\varphi_d,\theta_d}(r_d,\varphi_d,\theta_d)dr_d$$

$$= \int_0^R r_d^2 \sin\theta_d \frac{3}{4\pi R^3} dr_d$$

$$= \begin{cases} \frac{\sin\theta_d}{4\pi}, & \text{if } \theta_d \in (0,\pi], \varphi_d \in [-\pi,\pi) \\ 0, & \text{otherwise} \end{cases}$$

$$f^{(he)}_{\theta_d,\varphi_d}(\theta_d,\varphi_d) = \begin{cases} \frac{\sin\theta_d}{2\pi}, & \text{if } \theta_d \in (0,\pi], \varphi_d \in [0,\pi] \\ 0, & \text{otherwise.} \end{cases} \quad (21)$$

When either above bivariate 2-D-AOA distribution is nonzero, it is not a function of φ_d. Equation (21) shows θ_d is most probably near $\pi/2$, as expected because right above the mobile is where the scatterers are most probably located in the hemispheroid. The above-derived downlink 2-D-AOA's bivariate distribution concurs with that derived in [23], after adjustments between the different used coordinates.[6]

$$f^{(sp)}_{\theta_d}(\theta_d) = \begin{cases} \frac{1}{2}\sin\theta_d, & \text{if } \theta_d \in [0,\pi] \\ 0, & \text{otherwise} \end{cases}$$

$$= f^{(he)}_{\theta_d}(\theta_d) \quad (22)$$

which simply equals a π-multiple of (21).

VIII. Conclusion

This paper presents the open literature's first *analytically* derived *closed-form explicit* expressions of a landmobile cellular communication system's:

1) downlink trivariate distributions of the TOA and 2-D AOA;
2) uplink trivariate distributions of the TOA and 2-D AOA;
3) uplink bivariate distributions of the 2-D AOA;

in terms of the parameters of a geometric model relating the base station, the mobile, and scatterers.

References

[1] T. Aulin, "A modified model for the fading signal at a mobile radio channel," *IEEE Trans. Veh. Technol.*, vol. VT-28, pp. 182–203, Aug. 1979.

[2] J. D. Parsons and A. M. D. Turkmani, "Characterisation of mobile radio signals: model description," *Proc. Inst. Elect. Eng. Commun., Speech Vision*, vol. 138, no. 6, pt. I, pp. 549–556, Dec. 1991.

[3] A. M. D. Turkmani and J. D. Parsons, "Characterisation of mobile radio signals: base station crosscorrelation," *Proc. Inst. Elect. Eng. Commun., Speech Vision*, vol. 138, no. 6, pt. I, pp. 557–565, Dec. 1991.

[4] T. Kurner, D. J. Cichon, and W. Wiesbeck, "Evaluation and verification of the VHF/UHF propagation channel based on a 3-D-wave propagation model," *IEEE Trans. Antennas Propag.*, vol. 44, pp. 393–404, Mar. 1996.

[5] J. C. Liberti and T. S. Rappaport, "A geometrically based model for line-of-sight multipath radio channels," in *IEEE Veh. Technol. Conf.*, 1996, vol. 2, pp. 844–848.

[6] F. Vatalaro and A. Forcella, "Doppler spectrum in mobile-to-mobile communications in the presence of three-dimensional multipath scattering," *IEEE Trans. Veh. Technol.*, vol. 46, pp. 213–219, Feb. 1997.

[7] P. Petrus, J. H. Reed, and T. S. Rappaport, "Effects of directional antennas at the base station on the Doppler spectrum," *IEEE Commun. Lett.*, vol. 1, pp. 40–42, Mar. 1997.

[8] P. C. F. Eggers, "Generation of base station DOA distribution by Jacobi transformation of scattering areas," *Electron. Lett.*, vol. 34, no. 1, pp. 24–26, Jan. 8, 1998.

[9] O. Norklit and J. B. Andersen, "Diffuse channel model and experimental results for array antennas in mobile environments," *IEEE Trans. Antennas Propag.*, vol. 46, pp. 834–840, Jun. 1998.

[10] R. J. Piechocki, G. V. Tsoulos, and J. P. McGeehan, "Simple general formula for PDF of angle of arrival in large cell operational environments," *Electron. Lett.*, vol. 34, no. 18, pp. 1784–1785, Sep. 3, 1998.

[11] D. R. Van Rheeden and S. C. Gupta, "A geometric model for fading correlation in multipath radio channels," in *IEEE Int. Conf. Commun.*, 1998, vol. 3, pp. 1655–1659.

[12] S. Roy, "A three-dimensional wideband propagation model for the study of base station antenna arrays with application to LMCS," in *IEEE Veh. Technol. Conf.*, 1998, vol. 3, pp. 1805–1809.

[13] J. Laurila, A. F. Molisch, and E. Bonek, "Influence of the scatterer distribution on power delay profiles and azimuthal power spectra of mobile radio channels," in *Int. Symp. Spread Spectrum Technol. Applicat.*, 1998, vol. 1, pp. 267–271.

[14] S. Y.-D. Lien and M. Cherniakov, "Analytical approach for multipath delay spread power distribution," in *IEEE Global Telecommun. Conf.*, 1998, vol. 6, pp. 3680–3685.

[15] S. Qu and T. Yeap, "A three-dimensional scattering model for fading channels in land mobile environment," *IEEE Trans. Veh. Technol.*, vol. 48, pp. 765–781, May 1999.

[16] M. P. Lotter and P. van Rooyen, "Modeling spatial aspects of cellular CDMA/SDMA systems," *IEEE Commun. Lett.*, vol. 3, pp. 128–131, May 1999.

[17] R. Narasimban and D. C. Cox, "A generalized Doppler power spectrum for wireless environments," *IEEE Commun. Lett.*, vol. 3, pp. 164–165, Jun. 1999.

[18] R. B. Ertel and J. H. Reed, "Angle and time of arrival statistics for circular and elliptical scattering models," *IEEE J. Sel. Areas Commun.*, vol. 17, pp. 1829–1840, Nov. 1999.

[19] L. M. Correia, Ed., *Wireless Flexible Personalised Communication (COST 259: European Co-Operation in Mobile Radio Research)*. New York: Wiley, 2001.

[20] P. Petrus, J. H. Reed, and T. S. Rappaport, "Geometrical-based statistical macrocell channel model for mobile environments," *IEEE Trans. Commun.*, vol. 50, pp. 495–502, Mar. 2002.

[21] R. Janaswamy, "Angle and time of arrival statistics for the gaussian scatter density model," *IEEE Trans. Wireless Commun*, vol. 1, pp. 488–497, Jul. 2002.

[22] Y. Z. Mohasseb and M. P. Fitz, "A 3-D spatio-temporal simulation model for wireless channel," *IEEE J. Sel. Areas Commun.*, vol. 20, pp. 1193–1203, Aug. 2002.

[23] R. Janaswamy, "Angle of arrival statistics for a 3-D spheroid model," *IEEE Trans. Veh. Technol.*, vol. 51, pp. 1242–1247, Sep. 2002.

[24] A. Y. Olenko, K. T. Wong, and E. H.-O. Ng, "Analytically derived TOA-DOA statistics of uplink/downlink wireless multipaths arisen from scatterers on an hollow-disc around the mobile," *IEEE Antennas Wireless Propag. Lett.*, vol. 2, no. 22, pp. 345–348, 2003.

[25] Q. Yao and M. Patzold, "A novel 3-D spatial-temporal deterministic simulation model for mobile fading channels," in *IEEE Int. Symp. Personal, Indoor Mobile Radio Commun.*, 2003, vol. 2, pp. 1506–1520.

[26] A. F. Molisch, "A generic model for MIMO wireless propagation channels in macro- and microcells," *IEEE Trans. Signal Process.*, vol. 52, pp. 61–71, Jan. 2004.

[27] Y. Chen and V. K. Dubey, "Accuracy of geometric channel-modeling methods," *IEEE Trans. Veh. Technol.*, vol. 53, pp. 82–93, Jan. 2004.

[28] A. Y. Olenko, K. T. Wong, and M. Abdulla, "Analytically derived TOA-AOA distributions of uplink/downlink wireless-cellular multipaths arisen from scatterers with an inverted-parabolic spatial distribution around the mobile," *IEEE Signal Process. Lett.*, vol. 9, pp. 516–519, Jul. 2005.

[29] Q. Yao and M. Patzold, "Spatial-temporal characteristics of a half-spheroid model and its corresponding simulation model," in *IEEE Veh. Technol. Conf.*, Spring 2004, vol. 1, pp. 147–151.

[6]Reference [23] uses the coordinates in Fig. 2, whereas the derivation in this paper uses the coordinates in Fig. 1. The present coordinates allow the derivation of closed-form explicit expressions for the uplink's 2-D-AOA's joint bivariate distributions, as well as the uplink's and the downlink's trivariate TOA/2-D-AOA distributions.

Andriy Yakovych Olenko, photograph and biography not available at the time of publication.

Kainam Thomas Wong, photograph and biography not available at the time of publication.

Sajjad Ahmed Qasmi, photograph and biography not available at the time of publication.

Javad Ahmadi-Shokouh, photograph and biography not available at the time of publication.